DOI 10.52209/2706-977X_2025_2_72 **IRSTI 81.09.81** **UDC 620.1:667.621**

Selection of Geometric Parameters of Indenters that Provide Sufficient Sensitivity to Changes in Characteristics in the Volume of Material

Tursunov T.M.[1], Tursunov N.Q.[1], Kren A.P.[2], Urazbaev T.T.[1*], Ziyamukhamedova U. A.[1]
[1]Tashkent State Transport University, Tashkent, Uzbekistan
[2]State Scientific Institution «Institute of Applied Physics of the National Academy of Sciences of Belarus», Minsk, Belarus
*corresponding author

Abstract. This study investigates the selection of geometric parameters for indenters to ensure sufficient sensitivity in assessing the physical and mechanical properties of cast iron under dynamic loads. The research focuses on optimizing indenter dimensions (diameter, shape) and impact energy to achieve measurable plastic imprints while accounting for material heterogeneity, particularly graphite inclusions. Analytical and experimental approaches were used to evaluate the relationship between indenter geometry, deformation rates, and imprint characteristics. Results indicate that a spherical indenter with a diameter of 1.2 mm, mass of 5 g, and impact velocity of 3 m/s optimally balances imprint size (450–500 µm) and depth (50–120 µm) across cast iron hardness ranges (100–500 HBW). The findings highlight the importance of maintaining complete plasticity during indentation to minimize surface preparation effects and ensure reliable non-destructive testing. This work contributes to improved methodologies for dynamic hardness testing in industrial applications, particularly for high-strength cast irons.

Keywords: high-strength cast iron, hardness, induction crucible furnace, mechanical properties, indentation, impact, imprint.

Introduction

Cast iron casting is widely used in both domestic and foreign industrial enterprises. Cast iron is one of the main structural materials and is widely used in the automotive industry (for the production of cylinder blocks and crankshafts), rail transport (brake pads) [17], machine tool industry (machine bases) and the oil industry (pipes). Due to the presence of graphite inclusions, cast iron effectively dampens vibrations and can be used at low temperatures. However, when producing various products, there are difficulties with control, since it is often necessary not only to determine the structure of the cast iron (in particular, to distinguish between gray and high-strength), but also to accurately determine its physical and mechanical properties: strength, hardness and elastic modulus. If the problem of separating cast iron types can be solved using ultrasonic methods, then determining mechanical characteristics using non-destructive testing remains an urgent problem that needs to be solved. The structure of cast iron is very sensitive to various factors, such as the composition of the feedstock [18]. and the presence of components (including parasitic impurities, such as sulfur and sulfur compounds, even within the technical specifications) [11], alloying additives [24], as well as loading and mixing methods and heating conditions [13].

The situation in the field of cast iron materials science is unique: the industrial use of cast irons is ahead of the development of the theoretical foundations of their structure formation. Materials created experimentally often begin to be used before the theoretical justification for their production appears. This is especially true for new grades of cast iron, such as ADI, which have high strength (700-1450 MPa) and significant relative elongation at break.

Cast iron is a structurally heterogeneous material due to the presence of a large number of graphite inclusions, which can take various forms: lamellar (gray cast iron), spherical (high-strength), flake (malleable), there is also a vermicular form of graphite [1]. In addition to various forms of graphite, cast iron can have various bases: ferritic, ferritic-pearlite, pearlitic. White cast iron has a cementite structure. According to GOST 3443 "Cast iron castings with various forms of graphite. Methods for determining the structure" graphite inclusions can have sizes from 15 µm to 1000 µm [1]. It should be noted that large graphite inclusions sharply reduce mechanical properties and for products made of such cast iron, control of their characteristics, as a rule, is not carried out. The distribution of graphite in the cast iron structure can be both uniform and uneven, and also have a colonial, mesh and even branched distribution. The number of graphite inclusions is estimated by the average percentage of the area occupied on the microsection. For example, for lamellar graphite, the distribution density varies from 2 to 12%. Figure 1 shows the microstructure of real cast iron samples and an assessment of the distribution of characteristic sizes of various carbon inclusions.

Taking into account the above, for assessing the physical and mechanical characteristics of cast iron using the indentation method, the minimum sufficient linear size of the deformation region is about 500 µm with a hardness of about 100 HBW and 400-450 µm with a hardness of 500 HBW and more.

Cast iron is a critical structural material due to its vibration-damping properties and versatility. However, its heterogeneous structure, characterized by graphite inclusions (e.g., lamellar, spherical, vermicular), complicates non-destructive evaluation of mechanical properties like hardness, strength, and elastic modulus. While ultrasonic methods can distinguish between cast iron types (e.g., gray vs. high-strength), existing techniques fail to provide accurate, localized assessments of mechanical properties under dynamic loads, particularly for modern high-strength grades (e.g., ADI with 700–1450 MPa tensile strength). Current indentation methods lack systematic optimization of indenter geometry and loading parameters to ensure sensitivity across cast iron's hardness range (100–500 HBW). This limits their reliability in industrial settings, where dynamic loads and material heterogeneity demand precise control of deformation regimes (elastic-plastic vs. fully plastic).

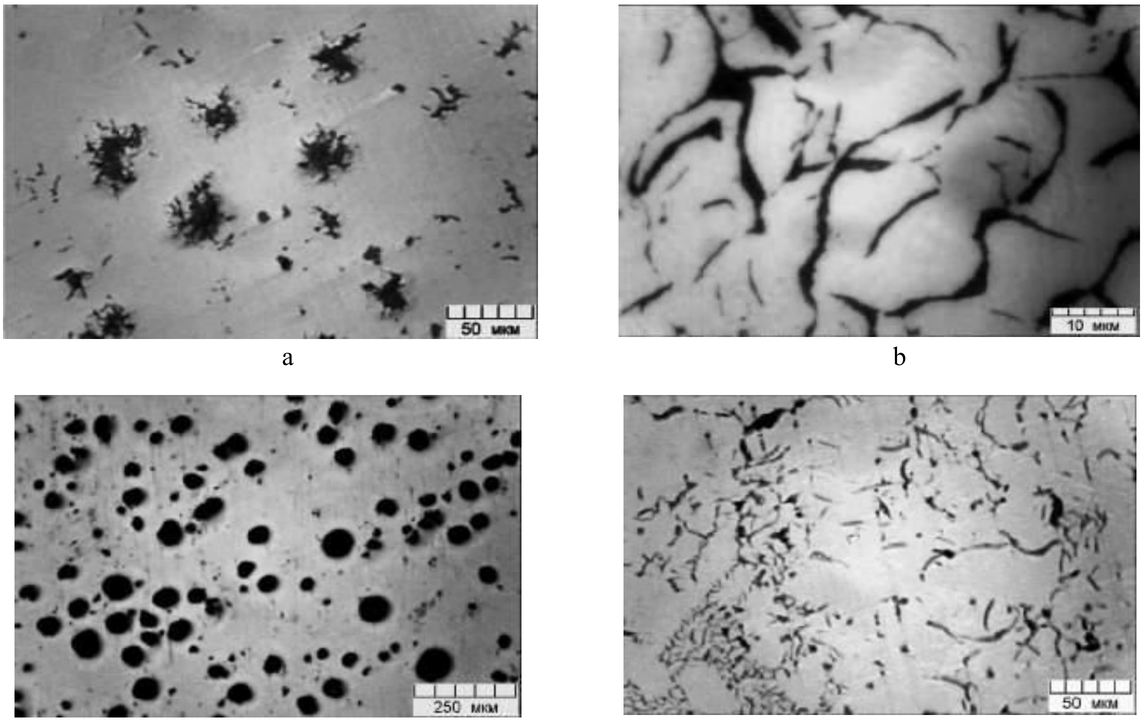

Fig.1. - Form of graphite (dark inclusions) in cast irons: a – flake-like, b – plate-like, c – spherical, d – vermicular

1. Methods

The brief analysis of the methods for determining the geometric and energy parameters of indentation shows that there is a need to solve the problem of selecting the optimal geometric and energy parameters of loading to create the required deformation of the material in order to reliably characterize its properties in a local volume and at the same time give its integral assessment.

To calculate the equivalent deformation during indentation, similar to that which will be formed during tension or compression of cast iron under uniaxial loading, and to obtain relationships linking the geometric parameters of the indenter and the created deformation value. The authors considered the process of elastic-plastic indentation. First, we will analyze the process of indentation of a sharp indenter in the form of a cone or a tetrahedral pyramid (Figure 2)

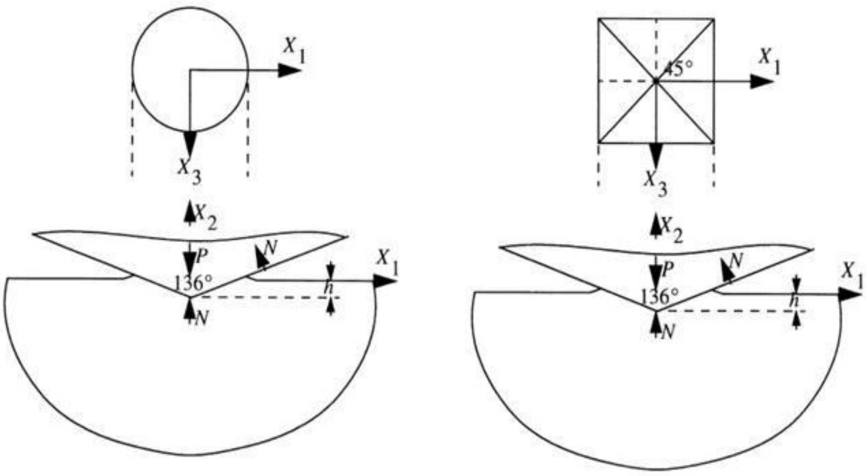

a b

N-reaction force, P-load force, h-penetration depth, X_i -direction of axes

Fig. 2. - Indentation of sharp indenters: cone (a) and pyramid (b)

When the elastic limit is first exceeded, the plastic zone is small and is completely covered by the material, which is in a purely elastic state, so that the plastic deformations have the same order of magnitude as the elastic ones. In this case, the displacement of the material by the indenter is compensated by elastic displacements of the environment. As the indentation depth increases, an increase in the pressure under the indenter is required to ensure the necessary expansion of the material. Eventually, the plastic zone reaches the free surface and the displaced material can freely flow plastically along the edges of the indenter. This becomes possible when the average pressure under the indenter P_m reaches a value determined by the theory of rigid-plastic media [2]:

$$P_m = C_k \cdot Y \tag{1}$$

where Y is the flow stress, and the value of Cк depends on the geometry of the indenter and is approximately equal to 3.0 in the state of complete plasticity.

According to [2], the flow state is achieved at pressure (1), where the constant C_k~1.1. There is an interval of intermediate values of the average contact pressure (from Y to 3Y), for which plastic flow is restrained by the surrounding elastic material, and deformation is carried out due to the radial expansion of the medium. From a practical point of view, three loading stages are of interest: elastic, elastic-plastic, and completely plastic. In [3], it was shown that the contact surface during indentation is covered by a hemispherical "core" of radius a (Figure 3).

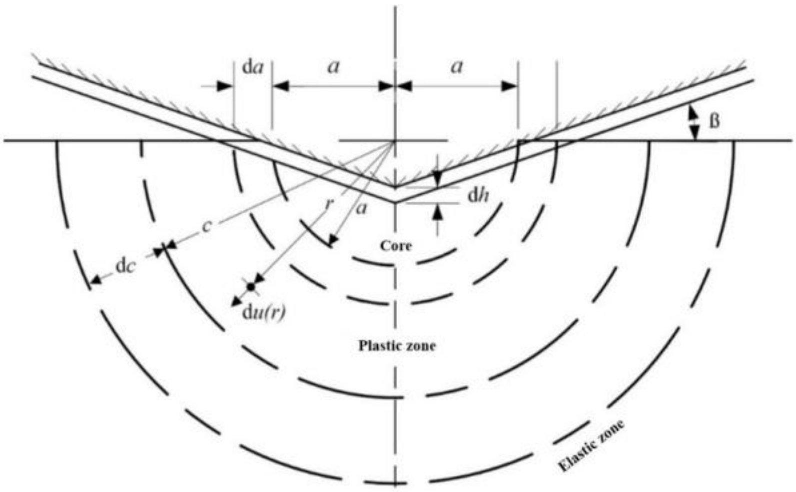

Fig.3. - Model with a spherical core for the analysis of the penetration of a cone into an elastic-plastic medium

A hydrostatic stress state of intensity $\bar{p}$ is formed inside the core. The elastic-plastic boundary is defined by the radius c, where c>a. The hydrostatic pressure in the core is equal to the radial component of the stress beyond the core boundary. It can also be argued that the radial displacement of particles lying on the boundary r=a, with an increase in the penetration depth dh, should be compensated by the material displaced by the indenter. If we follow the work [4], then the stresses in the plastic zone a ≤ r ≤ c are equal to:

$$\frac{\sigma_r}{Y} = -2\ln\left(\frac{c}{r}\right) - \frac{2}{3}, \tag{2a}$$

$$\frac{\sigma_\theta}{Y} = -2\ln\left(\frac{c}{r}\right) + \frac{1}{3}. \tag{2b}$$

In the elastic zone $r \geq c$:

$$\frac{\sigma_r}{Y} = -\frac{2}{3}\left(\frac{c}{r}\right)^3, \qquad \frac{\sigma_\theta}{Y} = \frac{1}{3}\left(\frac{c}{r}\right)^3. \tag{3}$$

The pressure in the core and the radial stress at the boundary of the core are equal:

$$\frac{\bar{p}}{Y} = -\frac{\sigma_r}{Y}\Big|_{r=a} = \frac{2}{3} + 2\ln\frac{c}{a} \tag{4}$$

Radial deformations are equal [4]:

$$\frac{du(r)}{dt} = \frac{Y}{E}\left[3(1-\nu)\left(\frac{c}{r}\right)^2 - 2(1-2\nu)\frac{r}{c}\right]. \tag{5}$$

From the condition of incompressibility of the core it follows that the expression found from this equation for c/a in (4) can be used to obtain the pressure in the core:

$$\frac{\bar{p}}{Y} = \frac{2}{3}\left[1 + \ln\left(\frac{1}{3}\frac{E\text{tg}\beta}{Y}\right)\right] \qquad (6)$$

where β – angle between the cone generatrix and the base surface ($\beta = \frac{\pi}{2} - \alpha$). At the same time $r=a$ and $dc/da = c/a$ =const.

From expression (6) it is evident that the hydrostatic pressure under the indenter is a function of the dimensionless variable $Etg\beta/Y$, which can be interpreted as the ratio of the deformation caused by the indenter ($tg\beta$) to the elastic deformability of the material (Y/E). In the case of a spherical indenter, it can be assumed that $tg\beta \approx \sin\beta = a/R$; the value of this ratio changes during penetration.

The penetration pressure under conditions of purely elastic, elastic-plastic and completely plastic states can be represented as a graph of the dependence of the dimensionless quantity P_m/Y on $E^*tg\beta/Y$, where "ß" is the angle of inclination of the indenter profile to the undeformed surface of the base at the edge of the contact area (Figure 4). This figure is based on data from [5-8].

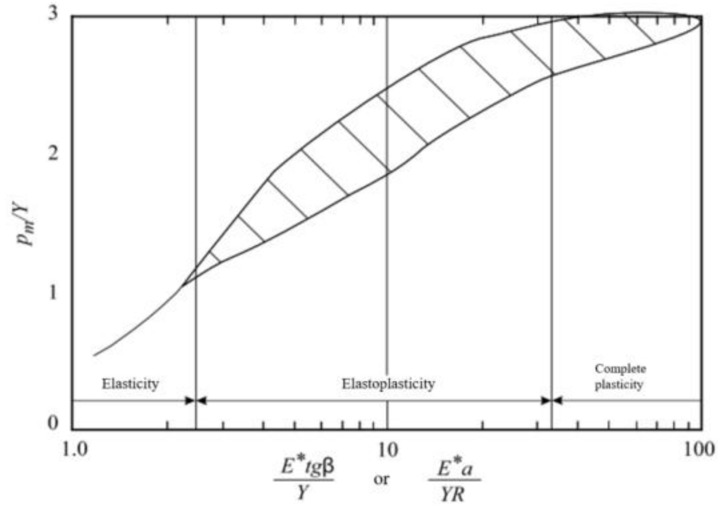

Fig.4. - Embedding of spheres and cones into an elastic-plastic half-space

The above results are valid for elastic-ideal-plastic bodies with a constant yield strength Y for uniaxial compression. Tabor [9] showed that the results for an ideal-plastic body can be applied with a good degree of approximation to bodies with hardening, for uniaxial compression upon reaching a deformation ε_R equal to $\varepsilon_R = 0{,}2tg\beta$.

For the Vickers pyramid, from here we have $\varepsilon_R \approx 0{,}07$. The theoretical calculations carried out are experimentally confirmed by the results of experiments carried out by Tabor and for a spherical indenter (Figure 5).

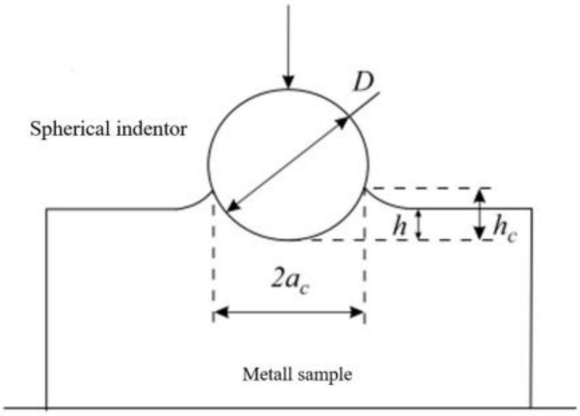

Fig.5. - Scheme of introduction of a spherical indenter

Following Meyer's work, which showed that the average contact pressure $P_m = K\left(\frac{a}{R}\right)^m$, Tabor proposed the concept of equivalent strain and stress. Based on Meyer's assumption that the index m is related to the strain hardening coefficient, Tabor assumed that the average pressure P_m in the state of full plasticity and the equivalent stress Y_r are proportional. The radius of the indentation a and the strain ε_r are also proportional:

$$Y_r = \psi\frac{P}{\pi a^2}, \qquad (7)$$
$$\varepsilon_r = \phi\frac{a}{R}.$$

To test these expressions, Tabor [9] conducted experiments that confirmed their correctness and obtained the following values of the coefficients: $\psi = 2{,}8 - 3{,}2$, $\phi = 0{,}2$.

Thus, the obtained expressions allow us to conclude that when deforming a material with a spherical indenter, the value of the equivalent deformation is equal to 0.2 *a/R* (or 0.2 *d/D*), and when indenting with a cone or pyramidal indenter, a constant deformation of about 7% will be created (when pressing in a Vickers pyramid).

2. Results

The results of calculating the pre-impact velocity of the indenter, as well as the dimensions of the imprint on materials with a hardness corresponding to the upper and lower limits of the range under consideration, are given in Tables 1 and 2.

The data in Tables 1 and 2 show that indenters with both 1 mm and 2 mm diameters are suitable for assessing the physical and mechanical properties of cast iron. For both indenter diameters, it is possible to select the impact energy that ensures the achievement of the required imprint diameter d_{min}. It should be noted that for an indenter with a diameter of 1 mm, the required value of d = 450 μm at a hardness of 500 HBW is ensured at an impact energy of 22 mJ. At the same time, at a hardness of 100 HBW with the same energy, the *d/D* ratio is 0.649. This value slightly exceeds the limits of inequality (10), but such an excess is acceptable. Therefore, it can be assumed that for an indenter with a diameter of 1 mm, the maximum indentation diameter at a hardness of 500 HBW is 450 μm. Using an indenter with a diameter of 2 mm allows increasing the indentation diameter on hard materials from 450 μm to 500 μm. However, this reduces the indentation depth by 40% (from 53.5 μm to 31.8 μm at a material hardness of 500 HBW and from 119.6 μm to 71 μm at a material hardness of 100 HBW). Since a decrease in the indentation depth will lead to an increase in the influence of the quality of the tested surface on the measurement results and, accordingly, will increase the labor intensity of preparing the product for testing, using an indenter with a diameter of 2 mm is impractical.

Table 1 - Calculation results for an indenter diameter of 1 mm

Hardness of material HBW	Diameter of the imprint d, μm	*d/D*	Depth of imprint h_c, μm	Impact energy, mJ	Pre-impact velocity V_{max}, m/s
500	500	0,5	67,0	34,6	3,7
	450	0,45	53,5	22,0	3,0
	400	0,4	41,7	13,4	2,3
100	714	0,71	150,0	34,6	3,7
	649	0,65	119,6	22,0	3,0
	582	0,58	93,3	13,4	2,3

Table 2 - Calculation results for an indenter diameter of 2 mm

Hardness of material HBW	Diameter of the imprint d, μm	*d/D*	Depth of imprint h_c, μm	Impact energy, mJ	Pre-impact Velocity V_{max}, m/s
500	500	0,25	31,8	15,5	2,5
	450	0,225	25,6	10,1	2,0
	400	0,2	20,2	6,3	1,6
100	740	0,37	71,0	15,5	2,5
	667	0,33	57,3	10,1	2,0
	594	0,3	45,2	6,3	1,6

At the same time, the use of indenters with a diameter in the range from 1 to 2 mm is of considerable interest. Unlike static hardness testers, this possibility is provided by portable devices implementing the dynamic indentation method: without being tied to standard diameters, it is possible to manufacture an indenter with any dimensions. Calculation of the pre-impact velocity of the indenter, as well as the dimensions of the imprint for nine variants of the indenter diameter (1.1; 1.2; … 1.9 mm) showed that the optimal option is to use an indenter with a diameter of 1.2 mm and a pre-impact velocity of 3 m/s. The results of the corresponding calculations are given in Table 3.

Table 3 – Calculation results for indenter diameter D=1.2 mm

Hardness of material HBW	Diameter of the imprint d, μm	*d/D*	Depth of imprint h_c, μm	Impact energy, mJ	Pre-impact Velocity V_{max}, m/s
500	480	0,4	50,1	23,2	3,0
100	698	0,58	112,0		

Comparing Tables 1.1 and 1.3, we can draw the following conclusions. Increasing the indenter diameter from 1 mm to 1.2 mm allows, at the same value of the pre-impact velocity, to increase the indentation diameter on hard materials from 450 μm to 480 μm. In this case, the ratio d/D does not exceed the limits of inequality (10), and the indentation depth decreases by only 6% (from 53.5 μm to 50.1 μm for a material hardness of 500 HBW and from 119.6 μm to 112 μm for a material hardness of 100 HBW). Thus, as a result of the analysis, it was established that the following indenter parameters are optimal for assessing the physical and mechanical properties of cast iron using the dynamic indentation method: weight - 5 g, diameter - 1.2 mm, pre-impact velocity - 3 m/s.

3. Discussion

In order to objectively characterize cast iron, one more condition must be met: the material must be in a state of complete plasticity. If this condition is met for a pyramid, then for a spherical indenter this means that the deformation must be in the range of $0.04<\varepsilon_r<0.12$, then the radius of the indentation must be $0.2R<a<0.6R$. In this case, the dependence of the average contact pressure on the applied force will take on a virtually constant value (Figure 6), which will allow us to further exclude the influence of the deformation value on the measured characteristics and take into account only the influence of the loading dynamics (deformation rate).

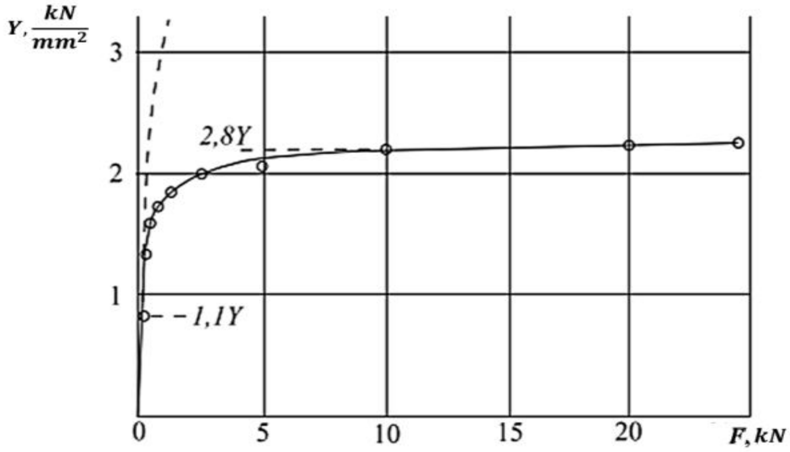

Fig. 6 - Dependence of average contact pressure on indentation force

The choice of the loading scheme for the studied cast irons with a hardness from 100 to 500 HBW consists of selecting the diameter of the spherical indenter D and the pre-impact speed of the indenter V_{max}, upon reaching which the diameter of the imprint will correspond to the minimum sufficient size of the deformation region (let us designate this diameter of the imprint as d_{min}). In addition, as established earlier, when measuring the physical and mechanical characteristics, the diameter of the imprint should be within the limits in the entire range of hardnesses of the tested cast irons:

$$0{,}2D < d < 0{,}6D \tag{8}$$

The value of the pre-impact velocity of the indenter Vmax, necessary to achieve the minimum sufficient diameter of the indentation dmin, can be determined from the law of conservation of energy, equating the kinetic energy of the falling indenter Wk and the energy of deformation of the material by the indenter Wд. The kinetic energy of the indenter of mass m is calculated using the formula:

$$W_{к} = \frac{1}{2} m V_{\max}^2. \tag{9}$$

The energy of deformation of the material during indentation is determined by integrating the dependence of the contact force on the depth of the indentation, which can be taken as linear in the first approximation:

$$W_{д} = \int_0^{hc} P dh = \frac{1}{2} P_{\max} h_c, \tag{10}$$

where h_c is the depth of the indentation,P_{max} is the maximum contact force.

The formula for determining the pre-impact velocity of the indenter obtained from expressions (8) and (9) is as follows:

$$V_{\max} = \sqrt{\frac{P_{\max} h_c}{m}}. \tag{11}$$

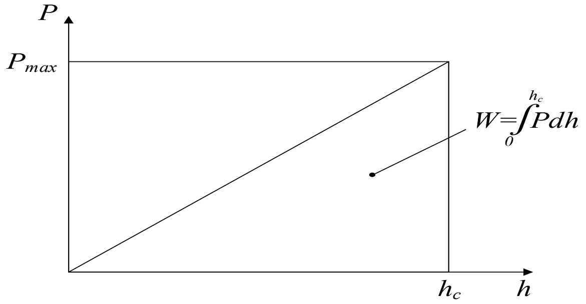

Fig.7 – Dependence of contact force on indentation depth

The depth of the indentation h_c can be determined through its diameter d from the equation obtained based on the indentation diagram (Figure 5) and given in STB ISO 6506-1-2022 "Metallic materials. Brinell hardness measurement. Part 1. Measurement method":

$$h_c = \frac{D}{2}\left(1 - \sqrt{1 - \frac{d^2}{D^2}}\right). \quad (12)$$

STB ISO 6506-1 establishes the relationship between the hardness of the test material HBW, the applied (contact) force F and the indentation diameter d:

$$HBW = 0{,}102 \frac{2P}{\pi D^2\left(1 - \sqrt{1 - \frac{d^2}{D^2}}\right)}. \quad (13)$$

Having solved this equation for the contact force, we obtain the value of the maximum contact force P at which the indentation diameter d on materials with different hardness reaches the required value (d_{min})

$$P_{\max} = \frac{HBW \cdot \pi D^2\left(1 - \sqrt{1 - \frac{d^2}{D^2}}\right)}{0{,}102 \cdot 2}. \quad (14)$$

As is known, with an increase in the hardness of the test material, the size of the imprint on its surface decreases (under the same impact conditions). Therefore, first of all, it is necessary to determine, based on the obtained equations, the impact energy and pre-impact velocity required to create a minimum sufficient imprint diameter d_{min} on products with a hardness corresponding to the upper limit of the range under consideration (500 HBW). Then, based on the impact energy obtained for this hardness, it is necessary to calculate the actual imprint diameter d on a material with a hardness corresponding to the lower limit of the range under consideration (100 HBW), and check that this diameter corresponds to inequality (8).

Conclusions

The paper shows that sharp indenters in the form of a Vickers pyramid and a cone create a constant deformation, the value of which is determined by the angle at the apex and a constant coefficient, the determination of which is possible based on the results of comparative tensile-compression tests of the material. When indenting with a sphere, the deformation value is a variable value and depends on the ratio of the imprint diameter to the indenter diameter. It is shown that it is optimal to use an indenter with a diameter of ~1 mm and a mass of ~5 g when indenting cast iron, which allows achieving a deformation in the range of up to 0.04-0.12 and a deformation rate of 1000-3000 1/s. At the same time, sufficient sensitivity to changes in mechanical characteristics under dynamic loads is ensured based on the size of graphite inclusions of no more than 500 μm.

References

[1] Anisovich A.G., Andrushkevich A.A. Microstructures of ferrous and non-ferrous metals. - Minsk: Belarusian Science, - 131 p. (2015)
[2] Johnson KL. Contact Mechanics. // Cambridge: Cambridge University Press.– P. 448-452. (1985)
[3] Boris Galanov, Sergei Ivanov, Valeriy Kartuzov. Improved core model of the indentation for the experimental determination // Mechanics of Materials,Volume 150. (November 2020, 103545)
[4] Houlsby, Guy T., and Alexander M. Puzrin. Advanced Plasticity Theories. Springer London, 2007.
[5] A.Kren, M. Delendik, A. Machikhin. Non-destructive evaluation of metal plasticity using a single impact microindentation // International Journal of Impact Engineering. – 2022– V.162. – P. 104141.
[6] Kral, E. R., K. Komvopoulos, and D. B. Bogy. "Elastic-plastic finite element analysis of repeated indentation of a half-space by a rigid sphere." (1993): 829-841.
[7] Richmond O., Morrison H. L., Devenpeck M. L. Sphere indentation with application to the Brinell hardness test. // Internat. J. Mech. Sci. № 16. – P. 75. (1974)

[8] A.P.Kren, A.S. Machikhin, A.Y. Marchenkov Impact indentation of metals in the transition region from the elastic to plastic state // Journal of Materials Science. – 2023. – № 58. – P. 961–970.
[9] Urazbayev, T., Tursunov, N., & Tursunov, T. (2024, March). Steel modification modes for improving the cast parts quality of the rolling stock couplers. In AIP Conference Proceedings (Vol. 3045, No. 1). AIP Publishing.
[10] Mamaev, S., Anna, A., Tursunov, S., Nigmatova, D., & Tursunov, T. (2023). Mathematical modeling of torsional vibrations of the wheel-motor unit of mains diesel locomotive UZTE16M. In E3S Web of Conferences (Vol. 401, p. 05014). EDP Sciences.
[11] Makhkamov, N. Y., Yusupov, G. U., Tursunov, T., & Djalilov, K. (2020, December). Properties of metal-based and nonmetal-based composite materials: A brief review. In IOP Conference Series: Earth and Environmental Science (Vol. 614, No. 1, p. 012068). IOP Publishing.
[12] Turakulov M., Tursunov N., Yunusov S. Steeling of synthetic cast iron in induction crucible furnace taking into account consumption rate of carburizers", E3S Web of Conferences 401, 05012 (2023). https://doi.org/10.1051/e3sconf/202340105012.
[13] Tokhir Tursunov, Nodirjon Tursunov and Talgat Urazbayev, "Investigation of heat exchange processes in the lining of induction furnaces", E3S Web of Conferences 401, 05029 (2023). https://doi.org/10.1051/e3sconf/202340105029.
[14] Turakulov M., Tursunov N., Yunusov S.New concept of cast iron melting technology in induction crucible furnace, E3S Web of Conferences 401, 01060 (2023). https://doi.org/10.1051/e3sconf/202340101060.
[15] Toirov O., Tursunov N. Efficiency of using heat-insulating mixtures to reduce defects of critical parts", E3S Web of Conferences 401, 05018 (2023). https://doi.org/10.1051/e3sconf/202340105018.
[16] Valieva D., Yunusov S., Tursunov N. Study of the operational properties of the bolster of a freight car bogie", E3S Web of Conferences 401, 05017 (2023). https://doi.org/10.1051/e3sconf/202340105017.
[17] Uchkun Rakhimov and Nodirjon Tursunov, "Development of technology for high-strength cast iron for manufacturing D49 head of cylinder", E3S Web of Conferences 401, 05013 (2023). https://doi.org/10.1051/e3sconf/202340105013.
[18] Suyunbayev, S., Khudayberganov, S., Jumayev, S., & Bashirova, A. (2024). Digital design trends of train and shunting operations at railway stations. In E3S Web of Conferences (Vol. 549, p. 04001). EDP Sciences. https://doi.org/10.1051/e3sconf/202454904001
[19] Jumayev S., Suyunbayev S., Sultanov T., Akhmedova M., Toxtakxodjaeva M. (2024). Enhancement of local traffic management systems using information technology. In E3S Web of Conferences (Vol. 583, p. 07016). EDP Sciences. https://doi.org/10.1051/e3sconf/202458307016
[20] Suyunbayev S., Khusenov U., Khudayberganov S. Sherzod Jumayev and Shokhrukh Kayumov. Improving use of shunting locomotives based on changes in infrastructure of railway station 05011 DOI: https://doi.org/10.1051/e3sconf/202336505011
[21] Fayzibaev, S., Ignotenko, O., & Urazbaev, T. (2021). Development of binding based on B-N-Ti-Al system compounds for creating a composite instrumental material for a final raining of railway parts. E3S Web of Conferences, 264. https://doi.org/10.1051/e3sconf/202126404073
[22] Fayzibayev S., Ignotenko O., Mamayev S., Urazbayev T., Nafasov, J. (2024). Development of a technique for the formation of Ti-Al system compounds under the influence of high pressures and temperatures. AIP Conference Proceedings, 3045(1). https://doi.org/10.1063/5.0197358
[23] Fayzibayev, S., Ignotenko, O., Urazbaev, T., Mamayev, S., & Nafasov, J. (2023). Development of technology for formation of AI-B-N system joints under influence of high pressures and temperatures to create composite tool material. E3S Web of Conferences, 401. https://doi.org/10.1051/e3sconf/202340105016
[24] Rakhimov U.T., Tursunov N.K.., Tursunov S.E. Improvement of production technology for spheroidal graphite cast iron with increased strength", AIP Conf. Proc. 3045, 060024 (2024). https://doi.org/10.1063/5.0197475.

Information of the authors

Tursunov Tokhir Muratovich, PhD, associate professor, Tashkent State Transport University
e-mail: t.tursunov87@gmail.com

Tursunov Nodirjon Kayumjonovich, DSc, professor, Tashkent State Transport University
e-mail: u_nadir@mail.ru

Kren Alexander Petrovich, DSc, professor, State Scientific Institution «Institute of Applied Physics of the National Academy of Sciences of Belarus»
e-mail: alekspk@mail.ru

Urazbaev Talgat Tileubaevich, PhD, associate professor, Tashkent State Transport University
e-mail: talgat_1988.26@mail.ru

Ziyamukhamedova Umida Alijonovna, DSc, professor, Tashkent State Transport University
e-mail: z.umida1973@yandex.ru